

Measurements of exclusive B_s^0 decays at the $\Upsilon(5S)$ resonance

A. Drutskoy,³ K. Abe,⁴² I. Adachi,⁸ H. Aihara,⁴⁴ D. Anipko,¹ A. M. Bakich,³⁹ E. Barberio,²⁰ I. Bedny,¹ U. Bitenc,¹³ I. Bizjak,¹³ S. Blyth,²³ A. Bondar,¹ M. Bračko,^{8,19,13} T. E. Browder,⁷ M.-C. Chang,⁴ P. Chang,²⁵ Y. Chao,²⁵ A. Chen,²³ K.-F. Chen,²⁵ W. T. Chen,²³ B. G. Cheon,⁶ R. Chistov,¹² Y. Choi,³⁸ J. Dalseno,²⁰ M. Danilov,¹² M. Dash,⁴⁷ J. Dragic,⁸ S. Eidelman,¹ S. Fratina,¹³ N. Gabyshev,¹ B. Golob,^{18,13} H. Ha,¹⁵ J. Haba,⁸ T. Hara,³¹ H. Hayashii,²² M. Hazumi,⁸ D. Heffernan,³¹ Y. Hoshi,⁴² W.-S. Hou,²⁵ Y. B. Hsiung,²⁵ K. Ikado,²¹ K. Inami,²¹ A. Ishikawa,⁴⁴ H. Ishino,⁴⁵ R. Itoh,⁸ M. Iwasaki,⁴⁴ Y. Iwasaki,⁸ J. H. Kang,⁴⁸ P. Kapusta,²⁶ H. Kawai,² T. Kawasaki,²⁸ H. J. Kim,¹⁶ H. O. Kim,³⁸ Y. J. Kim,⁵ K. Kinoshita,³ S. Korpar,^{19,13} P. Križan,^{18,13} P. Krokovny,⁸ R. Kulasiri,³ R. Kumar,³² C. C. Kuo,²³ A. Kuzmin,¹ Y.-J. Kwon,⁴⁸ M. J. Lee,³⁶ A. Limosani,⁸ S.-W. Lin,²⁵ D. Liventsev,¹² J. MacNaughton,¹⁰ G. Majumder,⁴⁰ T. Matsumoto,⁴⁶ S. McOnie,³⁹ W. Mitaroff,¹⁰ K. Miyabayashi,²² H. Miyata,²⁸ Y. Miyazaki,²¹ G. R. Moloney,²⁰ E. Nakano,³⁰ M. Nakao,⁸ Z. Natkaniec,²⁶ S. Nishida,⁸ S. Ogawa,⁴¹ T. Ohshima,²¹ S. Okuno,¹⁴ S. L. Olsen,⁷ Y. Onuki,³⁴ H. Ozaki,⁸ P. Pakhlov,¹² G. Pakhlova,¹² R. Pestotnik,¹³ L. E. Piilonen,⁴⁷ Y. Sakai,⁸ N. Satoyama,³⁷ T. Schietinger,¹⁷ O. Schneider,¹⁷ J. Schümann,⁸ A. J. Schwartz,³ R. Seidl,^{9,34} K. Senyo,²¹ M. E. Sevier,²⁰ M. Shapkin,¹¹ H. Shibuya,⁴¹ J. B. Singh,³² A. Somov,³ N. Soni,³² S. Stanič,²⁹ M. Starič,¹³ H. Stoeck,³⁹ K. Sumisawa,⁸ T. Sumiyoshi,⁴⁶ S. Suzuki,³⁵ F. Takasaki,⁸ K. Tamai,⁸ M. Tanaka,⁸ G. N. Taylor,²⁰ Y. Teramoto,³⁰ X. C. Tian,³³ I. Tikhomirov,¹² S. Uehara,⁸ K. Ueno,²⁵ Y. Unno,⁶ S. Uno,⁸ Y. Ushiroda,⁸ Y. Usov,¹ G. Varner,⁷ S. Villa,¹⁷ A. Vinokurova,¹ C. H. Wang,²⁴ Y. Watanabe,⁴⁵ J. Wicht,¹⁷ B. D. Yabsley,³⁹ A. Yamaguchi,⁴³ Y. Yamashita,²⁷ M. Yamauchi,⁸ V. Zhilich,¹ V. Zhulanov,¹ and A. Zupanc¹³

(Belle Collaboration)

¹*Budker Institute of Nuclear Physics, Novosibirsk*²*Chiba University, Chiba*³*University of Cincinnati, Cincinnati, Ohio 45221*⁴*Department of Physics, Fu Jen Catholic University, Taipei*⁵*The Graduate University for Advanced Studies, Hayama*⁶*Hanyang University, Seoul*⁷*University of Hawaii, Honolulu, Hawaii 96822*⁸*High Energy Accelerator Research Organization (KEK), Tsukuba*⁹*University of Illinois at Urbana-Champaign, Urbana, Illinois 61801*¹⁰*Institute of High Energy Physics, Vienna*¹¹*Institute of High Energy Physics, Protvino*¹²*Institute for Theoretical and Experimental Physics, Moscow*¹³*J. Stefan Institute, Ljubljana*¹⁴*Kanagawa University, Yokohama*¹⁵*Korea University, Seoul*¹⁶*Kyungpook National University, Taegu*¹⁷*Swiss Federal Institute of Technology of Lausanne, EPFL, Lausanne*¹⁸*University of Ljubljana, Ljubljana*¹⁹*University of Maribor, Maribor*²⁰*University of Melbourne, School of Physics, Victoria 3010*²¹*Nagoya University, Nagoya*²²*Nara Women's University, Nara*²³*National Central University, Chung-li*²⁴*National United University, Miao Li*²⁵*Department of Physics, National Taiwan University, Taipei*²⁶*H. Niewodniczanski Institute of Nuclear Physics, Krakow*²⁷*Nippon Dental University, Niigata*²⁸*Niigata University, Niigata*²⁹*University of Nova Gorica, Nova Gorica*³⁰*Osaka City University, Osaka*³¹*Osaka University, Osaka*³²*Panjab University, Chandigarh*³³*Peking University, Beijing*³⁴*RIKEN BNL Research Center, Upton, New York 11973*³⁵*Saga University, Saga*³⁶*Seoul National University, Seoul*

³⁷*Shinshu University, Nagano*³⁸*Sungkyunkwan University, Suwon*³⁹*University of Sydney, Sydney, New South Wales*⁴⁰*Tata Institute of Fundamental Research, Mumbai*⁴¹*Toho University, Funabashi*⁴²*Tohoku Gakuin University, Tagajo*⁴³*Tohoku University, Sendai*⁴⁴*Department of Physics, University of Tokyo, Tokyo*⁴⁵*Tokyo Institute of Technology, Tokyo*⁴⁶*Tokyo Metropolitan University, Tokyo*⁴⁷*Virginia Polytechnic Institute and State University, Blacksburg, Virginia 24061*⁴⁸*Yonsei University, Seoul*

(Received 26 March 2007; published 12 July 2007)

Several exclusive B_s^0 decays are studied using a 1.86 fb^{-1} data sample collected at the $Y(5S)$ resonance with the Belle detector at the KEKB asymmetric energy e^+e^- collider. In the $B_s^0 \rightarrow D_s^- \pi^+$ decay mode we find 10 B_s^0 candidates and measure the corresponding branching fraction. Combining the $B_s^0 \rightarrow D_s^{(*)-} \pi^+$, $B_s^0 \rightarrow D_s^{(*)-} \rho^+$, $B_s^0 \rightarrow J/\psi \phi$, and $B_s^0 \rightarrow J/\psi \eta$ decay modes, a significant B_s^0 signal is observed. The ratio $\sigma(e^+e^- \rightarrow B_s^* \bar{B}_s^*)/\sigma(e^+e^- \rightarrow B_s^{(*)} \bar{B}_s^{(*)}) = (93_{-9}^{+7} \pm 1)\%$ is obtained at the $Y(5S)$ energy, indicating that B_s^0 meson production proceeds predominantly through the creation of $B_s^* \bar{B}_s^*$ pairs. The B_s^0 and B_s^* meson masses are measured to be $M(B_s^0) = (5370 \pm 1 \pm 3) \text{ MeV}/c^2$ and $M(B_s^*) = (5418 \pm 1 \pm 3) \text{ MeV}/c^2$. Upper limits on the $B_s^0 \rightarrow \gamma\gamma$, $B_s^0 \rightarrow \phi\gamma$, $B_s^0 \rightarrow K^+K^-$, and $B_s^0 \rightarrow D_s^{(*)+} D_s^{(*)-}$ branching fractions are also reported.

DOI: [10.1103/PhysRevD.76.012002](https://doi.org/10.1103/PhysRevD.76.012002)

PACS numbers: 13.25.Gv, 13.25.Hw, 14.40.Gx, 14.40.Nd

I. INTRODUCTION

A considerable B_s^0 production rate has been recently measured in e^+e^- collisions at the energy of the $Y(5S)$ resonance [1,2]. Thus, high luminosity e^+e^- B -factories have great potential for studies of exclusive B_s^0 decays. Although several B_s^0 decay channels have been recently observed by the Tevatron experiments [3,4], a number of B_s^0 decay modes can be better measured at e^+e^- colliders running at the $Y(5S)$ energy. The detectors taking data at the $Y(5S)$ have many advantages in studies of B_s^0 decays, such as high photon and π^0 reconstruction efficiency, trigger efficiency of almost 100% for hadronic modes, and excellent charged kaon and pion identification. The possibility of partial reconstruction of specific B_s^0 decays and a model-independent determination of the number of initial B_s^0 mesons, which opens the possibility of precise absolute B_s^0 branching fraction measurements, are additional advantages of B_s^0 studies at e^+e^- colliders running at the $Y(5S)$.

In this paper we report measurements of exclusive B_s^0 decays based on an $Y(5S)$ data sample of 1.86 fb^{-1} , collected with the Belle detector [5] at the KEKB asymmetric energy e^+e^- collider [6]. This data sample is more than 4 times larger than the 0.42 fb^{-1} dataset collected at the $Y(5S)$ by the CLEO experiment in 2003 [7], where first evidence of exclusive B_s^0 decays at the $Y(5S)$ was found.

We fully reconstruct six modes $B_s^0 \rightarrow D_s^- \pi^+$, $B_s^0 \rightarrow D_s^{*-} \pi^+$, $B_s^0 \rightarrow D_s^- \rho^+$, $B_s^0 \rightarrow D_s^{*-} \rho^+$, $B_s^0 \rightarrow J/\psi \phi$, and $B_s^0 \rightarrow J/\psi \eta$, which have large reconstruction efficiencies and are mediated by unsuppressed $b \rightarrow c$ tree diagrams. Charge-conjugate modes are implicitly included everywhere in this paper. To improve the statistical significance

of the B_s^0 signal, these six modes are combined; the masses of the B_s^0 and B_s^* mesons are determined from a common signal fit.

In addition, we search for several rare B_s^0 decays: the penguin annihilation decay $B_s^0 \rightarrow \gamma\gamma$, the electromagnetic $b \rightarrow s$ penguin decay $B_s^0 \rightarrow \phi\gamma$, and the hadronic $b \rightarrow s$ penguin decay $B_s^0 \rightarrow K^+K^-$. Although the branching fractions for these decays are expected to be too small to be observed with this dataset, we can obtain useful upper limits. To date, only upper limits for the decays $B_s^0 \rightarrow \gamma\gamma$ [8] and $B_s^0 \rightarrow \phi\gamma$ [9] have been published. Within the standard model (SM) the $B_s^0 \rightarrow \gamma\gamma$ decay is expected to proceed via a penguin annihilation diagram and to have a branching fraction in the range $(0.5 - 1.0) \times 10^{-6}$ [10,11]. However, this decay is sensitive to some beyond-the-standard model (BSM) contributions and can be enhanced by one to 2 orders of magnitude in some BSM models [12,13]. Although current measurements of the process $B \rightarrow X_s \gamma$ provide a more restrictive constraint for many BSM models, in these models the $B_s^0 \rightarrow \gamma\gamma$ process is more sensitive.

The decay modes $B_s^0 \rightarrow \phi\gamma$ and $B_s^0 \rightarrow K^+K^-$ are also mediated by penguin diagrams; these decays are natural processes in which to search for BSM physics [14–18]. The decay $B_s^0 \rightarrow K^+K^-$ has been observed by CDF using a simultaneous multichannel analysis [19], where overlapping signal peaks from the $B_s^0 \rightarrow K^+K^-$, $B^0 \rightarrow K^+\pi^-$, $B^0 \rightarrow \pi^+\pi^-$, and $B_s^0 \rightarrow K^-\pi^+$ decay modes were separated statistically in the fit. In this analysis the ratio $(f_s^T/f_d^T) \times \mathcal{B}(B_s^0 \rightarrow K^+K^-)/\mathcal{B}(B^0 \rightarrow K^+\pi^-) = 0.46 \pm 0.08 \pm 0.07$ was obtained, where (f_s^T/f_d^T) is the ratio of production fractions of B_s^0 and B^0 at Tevatron center-of-mass energy $\sqrt{s} = 1.96 \text{ TeV}$.

We have also searched for the $B_s^0 \rightarrow D_s^{(*)+} D_s^{(*)-}$ decay modes. These decay branching fractions are of special interest [20,21]. These modes are expected to be predominantly CP eigenstates and, because their branching fractions are expected to be large, they should lead to a sizable lifetime difference between the CP -odd and CP -even B_s^0 mesons. Therefore within the SM framework the relative decay-width difference $\Delta\Gamma_{B_s^0}/\Gamma_{B_s^0}$ can be obtained from measurement of the $B_s^0 \rightarrow D_s^{(*)+} D_s^{(*)-}$ branching fractions. The first observation of the $B_s^0 \rightarrow D_s^+ D_s^-$ decay has recently been published by the CDF collaboration [22].

II. BELLE DETECTOR AND EVENT SELECTION

The Belle detector operates at KEKB [6], an asymmetric energy double storage ring designed to collide 8 GeV electrons and 3.5 GeV positrons to produce $Y(4S)$ mesons with a boost of $\beta\gamma = 0.425$. In this analysis we use a data sample of 1.86 fb^{-1} taken at the $Y(5S)$ energy of $\sim 10869 \text{ MeV}$ with the same boost. The experimental conditions for data taking at the $Y(5S)$ were identical to those for $Y(4S)$ or continuum running.

The Belle detector is a general-purpose large-solid-angle magnetic spectrometer that consists of a silicon vertex detector, a central drift chamber (CDC), an array of aerogel threshold Čerenkov counters (ACC), a barrel-like arrangement of time-of-flight scintillation counters (TOF), and an electromagnetic calorimeter comprised of CsI(Tl) crystals (ECL) located inside a superconducting solenoidal coil with a 1.5 T magnetic field. An iron flux-return located outside the coil is instrumented to detect K_L^0 mesons and to identify muons (KLM). The detector is described in detail elsewhere [5]. A GEANT-based detailed simulation of the Belle detector is used to produce Monte Carlo event samples (MC) and determine efficiencies.

Charged tracks are required to have momenta greater than $100 \text{ MeV}/c$. Kaon and pion mass hypotheses are assigned based on a likelihood ratio $\mathcal{L}_{K/\pi} = \mathcal{L}_K/(\mathcal{L}_K + \mathcal{L}_\pi)$, obtained by combining information from the CDC (dE/dx), ACC, and TOF systems. We require $\mathcal{L}_{K/\pi} > 0.6$ ($\mathcal{L}_{K/\pi} < 0.6$) for kaon (pion) candidates [23]. With these requirements, the identification efficiency for particles used in this analysis varies from 86% to 91% (94% to 98%) for kaons (pions). A tighter kaon identification requirement $\mathcal{L}_{K/\pi} > 0.8$ is applied for the $B_s^0 \rightarrow K^+ K^-$ decay, where the pion misidentification background is large.

Electrons are identified by combining information from the CDC (specific ionization dE/dx), the ACC, and the ECL (electromagnetic shower position, shape, and energy) [24]. Muons are identified by matching tracks to KLM hits and by using penetration depth information [25].

ECL clusters with a photonlike shape that are not associated with charged tracks are accepted as photon candi-

dates. Primary candidate photons (γ) that are used to reconstruct the $B_s^0 \rightarrow \phi\gamma$ and $B_s^0 \rightarrow \gamma\gamma$ decays are required to have proper bunch-crossing timing and to lie within the acceptance of the ECL barrel ($33^\circ < \theta_\gamma < 128^\circ$). To reduce the background from high-energy π^0 decays where the two daughter photons have merged into a single cluster in the calorimeter, the ECL energy deposition in a group of 3×3 cells is required to exceed 95% of that in the group of 5×5 cells around the maximum energy cell. The main background sources of high-energy photons are $\pi^0 \rightarrow \gamma\gamma$ and $\eta \rightarrow \gamma\gamma$ decays. To reduce these backgrounds, restrictions are imposed on the invariant mass of the candidate primary photon and any other photon (γ') in the event. The primary photon is rejected if $120 \text{ MeV}/c^2 < M(\gamma\gamma') < 145 \text{ MeV}/c^2$ and $E_{\gamma'} > 30 \text{ MeV}$, or if $510 \text{ MeV}/c^2 < M(\gamma\gamma') < 570 \text{ MeV}/c^2$ and $E_{\gamma'} > 200 \text{ MeV}$.

Neutral pion candidates are formed from pairs of photons, each with energy greater than 150 MeV ; the photons must have an invariant mass within $\pm 15 \text{ MeV}/c^2$ of the nominal π^0 mass (i.e. $\sim 3\sigma$, where $\sigma \sim 5 \text{ MeV}/c^2$ is the π^0 mass resolution). A mass-constrained kinematic fit is performed on the π^0 candidates to improve their energy resolution. We reconstruct η mesons only in the clean $\eta \rightarrow \gamma\gamma$ mode, requiring an invariant mass within $\pm 20 \text{ MeV}/c^2$ ($\sim 2\sigma$) of the nominal η mass and photon energies larger than 50 MeV . K_S^0 candidates are formed from $\pi^+ \pi^-$ pairs with an invariant mass within $\pm 10 \text{ MeV}/c^2$ ($\sim 3\sigma$) of the nominal K_S^0 mass and having a common vertex displaced from the interaction point by more than 0.1 cm in the plane perpendicular to the beam direction.

The invariant mass for $K^{*0} \rightarrow K^+ \pi^-$ candidates is required to be within $\pm 50 \text{ MeV}/c^2$ of the nominal K^{*0} mass; those of $\phi \rightarrow K^+ K^-$ candidates, within $\pm 12 \text{ MeV}/c^2$ of the ϕ mass. A $\pm 100 \text{ MeV}/c^2$ mass window is used to select $\rho^+ \rightarrow \pi^+ \pi^0$ candidates. D_s^- mesons are reconstructed in the $\phi\pi^-$, $K^{*0}K^-$, and $K_S^0K^-$ decay channels; all candidates must have a mass within $\pm 12 \text{ MeV}/c^2$ ($\sim 2.5\sigma$) of the nominal D_s^- mass. The D_s^- helicity angle distributions are expected to be proportional to $\cos^2\theta_{\text{hel}}^{D_s^-}$ for pseudoscalar-vector final states; thus a $|\cos\theta_{\text{hel}}^{D_s^-}| > 0.25$ requirement is applied for the $D_s^- \rightarrow \phi\pi^-$ and $D_s^- \rightarrow K^{*0}K^-$ decays. The helicity angle $\theta_{\text{hel}}^{D_s^-}$ is defined as the angle between the directions of the K^- and D_s^- momenta in the ϕ rest frame (or the directions of the π^- and D_s^- momenta in the K^{*0} rest frame in the case of $K^{*0}K^-$ decay).

D_s^{*-} candidates are reconstructed in the $D_s^{*-} \rightarrow D_s^- \gamma$ mode; the measured D_s^{*-} and D_s^- mass difference is required to be within $\pm 10 \text{ MeV}/c^2$ of its nominal value. The invariant mass of candidate J/ψ mesons is required to satisfy $|M(\mu^+ \mu^-) - m_{J/\psi}| < 30 \text{ MeV}/c^2$ for the muon decay mode and to satisfy $-100 \text{ MeV}/c^2 < M(e^+ e^-) - m_{J/\psi} < 30 \text{ MeV}/c^2$ for the electron decay mode, where $m_{J/\psi}$ is the nominal J/ψ mass.

B_s^0 decays are reconstructed in the following final states: $D_s^- \pi^+$, $D_s^- \rho^+$, $D_s^{*-} \pi^+$, $D_s^{*-} \rho^+$, $J/\psi \phi$, $J/\psi \eta$, $D_s^{(*)+} D_s^{(*)-}$, $K^+ K^-$, $\phi \gamma$, and $\gamma \gamma$. The signals can be observed using two variables: the energy difference $\Delta E = E_{B_s^0}^{\text{CM}} - E_{\text{beam}}^{\text{CM}}$ and the beam-energy-constrained mass $M_{\text{bc}} = \sqrt{(E_{\text{beam}}^{\text{CM}})^2 - (p_{B_s^0}^{\text{CM}})^2}$, where $E_{B_s^0}^{\text{CM}}$ and $p_{B_s^0}^{\text{CM}}$ are the energy and momentum of the B_s^0 candidate in the $e^+ e^-$ center-of-mass (CM) system, and $E_{\text{beam}}^{\text{CM}}$ is the CM beam energy. The B_s^0 mesons can be produced in $e^+ e^-$ collisions at the $\Upsilon(5S)$ energy via intermediate $B_s^* \bar{B}_s^*$, $B_s^* \bar{B}_s^0$, $B_s^0 \bar{B}_s^*$, and $B_s^0 \bar{B}_s^0$ channels, with $B_s^* \rightarrow B_s^0 \gamma$. These intermediate channels can be distinguished kinematically in the M_{bc} and ΔE plane, where three well-separated B_s^0 signal regions can be defined corresponding to the cases where both, only one, or neither of the B_s^0 mesons originate from a B_s^* decay. The events obtained from MC simulation of the $B_s^0 \rightarrow D_s^- \pi^+$ decay are shown in Fig. 1 for the intermediate $\Upsilon(5S)$ decay channels $B_s^* \bar{B}_s^*$, $B_s^* \bar{B}_s^0$, $B_s^0 \bar{B}_s^*$, and $B_s^0 \bar{B}_s^0$. The signal regions are defined as ellipses corresponding to $\pm(2.0\text{--}2.5)\sigma$ (i.e. 95–98% acceptance) resolution intervals in M_{bc} and ΔE . The signal events from the different intermediate channels are well-separated in the M_{bc} and ΔE plane. MC simulation shows that the separation between the channels in the M_{bc} projection is $\sim 3\sigma$ or better for all studied B_s^0 decays. Elliptical regions do not describe well the signal shape in the case of B_s^0 decays to the final

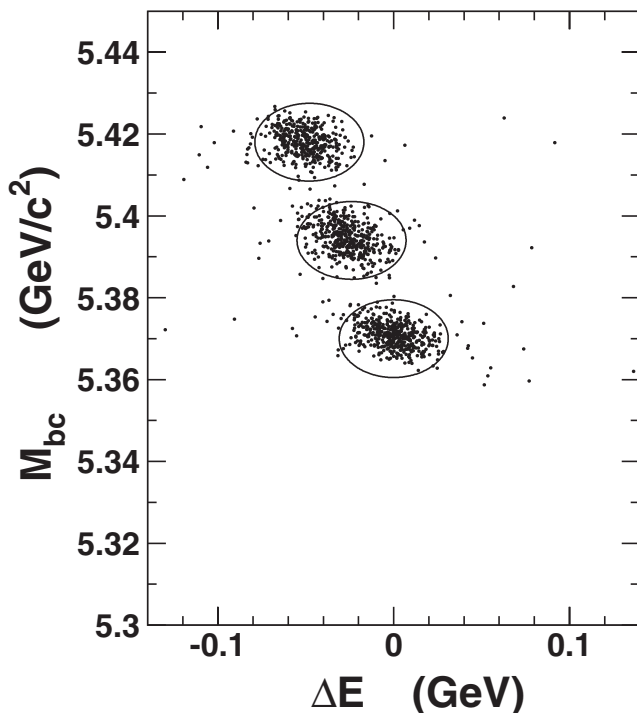


FIG. 1. The M_{bc} and ΔE scatter plot for the $B_s^0 \rightarrow D_s^- \pi^+$ decay obtained from the MC simulation. The ellipses show the signal regions for the intermediate $B_s^* \bar{B}_s^*$ (top elliptical region), $B_s^* \bar{B}_s^0$ and $B_s^0 \bar{B}_s^*$ (middle elliptical region), and $B_s^0 \bar{B}_s^0$ (bottom elliptical region) channels.

states with photons or electrons, because the radiative energy losses result in a long tail on the left side of the signal ΔE distribution. In such decay modes the acceptance of the elliptical signal regions decreases to (70–80)%. A MC simulation indicates that the correlation between the M_{bc} and ΔE variables is small and can be neglected in this analysis. The numbers of events inside and outside these elliptical regions can be used to estimate the number of B_s^0 signal and background events.

After all selections the dominant background is from $e^+ e^- \rightarrow q \bar{q}$ continuum events ($q = u, d, s, \text{ or } c$). Topologically, B_s^0 events are expected to be spherical, whereas continuum events are expected to be jetlike. To suppress continuum background, we apply topological cuts. These were optimized using MC to model the signal and data outside the B_s^0 signal regions to estimate background. The ratio of the second to the zeroth Fox-Wolfram moments [26] is required to be less than 0.3 for the high background $D_s^{(*)-} \pi^+$, $D_s^{(*)-} \rho^+$, and $K^+ K^-$ final states, less than 0.5 for the $\gamma \gamma$ final state (to increase the signal efficiency of such nonspherical B_s^0 decays), and less than 0.4 for all the other final states. To suppress continuum further, the angle θ_{thr}^* in the CM between the thrust axis of the particles forming the B_s^0 candidate and the thrust axis of all other particles in the event is used. We require $|\cos \theta_{\text{thr}}^*| < 0.9$ for the low background final states with a J/ψ , $|\cos \theta_{\text{thr}}^*| < 0.7$ for the $D_s^{(*)-} \rho^+$ final states, $|\cos \theta_{\text{thr}}^*| < 0.6$ for B_s^0 events reconstructed using the $D_s^- \rightarrow K^{*0} K^-$ decay mode, $|\cos \theta_{\text{thr}}^*| < 0.5$ for the very high background $K^+ K^-$ final state, and $|\cos \theta_{\text{thr}}^*| < 0.8$ for all the other final states.

More than one B_s^0 candidate per event can be selected. Using MC simulation we find that B_s^0 decays to channels with D_s^- or D_s^{*-} mesons can produce incorrect candidates reconstructed in a cross-channel. Because the photon from the $D_s^{*-} \rightarrow D_s^- \gamma$ decay has a low energy, this photon can be removed from the B_s^0 reconstruction resulting in the replacement of an original D_s^{*-} by its daughter D_s^- or, conversely, an original D_s^- meson can be combined with a random photon to produce a false D_s^{*-} candidate. For example, every $B_s^0 \rightarrow D_s^{*-} \pi^+$ decay will produce an incorrect $B_s^0 \rightarrow D_s^- \pi^+$ candidate and $\sim 37\%$ of $B_s^0 \rightarrow D_s^- \pi^+$ decays will produce incorrect $B_s^0 \rightarrow D_s^{*-} \pi^+$ candidates. Moreover, multiple candidates can be reconstructed in the $B_s^0 \rightarrow D_s^{*-} \pi^+$ decay mode if the original photon from the D_s^{*-} decay is replaced by a random photon that satisfies the D_s^{*-} mass window requirement. The M_{bc} distribution of incorrectly reconstructed B_s^0 candidates has the same central value as the original signal, but the width is slightly larger. However, the ΔE distribution of these incorrectly reconstructed B_s^0 candidates is (200–300) MeV wide and shifted to negative values if the correct photon is lost and to positive values when a random photon is added.

We checked the effects of incorrectly reconstructed B_s^0 candidates on the results of the measurements reported in

this paper. Because of the large spread in the ΔE distribution of the incorrectly reconstructed candidates and the low statistics used in this analysis, these effects are found to be small and are neglected; the corresponding uncertainties are included in the systematic error. We also checked other sources of multiple candidates in all studied decay modes and found that these effects can be neglected in the M_{bc} and ΔE measurements presented below. It should be noted that the MC efficiency calculations also include multiple candidates and, therefore, a corresponding correction for this effect is applied.

III. STUDY OF $B_s^0 \rightarrow D_s^{(*)-} \pi^+$, $B_s^0 \rightarrow D_s^{(*)-} \rho^+$, $B_s^0 \rightarrow J/\psi \phi$, AND $B_s^0 \rightarrow J/\psi \eta$ DECAYS

The M_{bc} versus ΔE distribution for the $B_s^0 \rightarrow D_s^- \pi^+$ candidates is shown in Fig. 2(a). Nine events are observed within the elliptical signal region corresponding to the $B_s^* \bar{B}_s^*$ pair production channel. Only one event is observed in the signal region for the $B_s^* \bar{B}_s^0 + B_s^0 \bar{B}_s^*$ channels, and no events are observed for the $B_s^0 \bar{B}_s^0$ channel. Background outside the signal regions is small and corresponds to ~ 0.1 events in each of the three signal regions. The total number of $b\bar{b}$ events in the sample and the fraction of $B_s^{(*)} \bar{B}_s^{(*)}$ events among all $b\bar{b}$ events at the $Y(5S)$ have been determined in [2] to be $N_{5S}^{b\bar{b}} = (5.61 \pm 0.03_{\text{stat}} \pm 0.29_{\text{sys}}) \times 10^5$ and $f_s = (18.0 \pm 1.3 \pm 3.2)\%$, respectively. We assume that 100% of B_s^* mesons decay to the ground state B_s . From the 10 observed events, the background estimate of 0.3 events, and the full reconstruction efficiency of $(0.71 \pm 0.10)\%$ (intermediate branching fractions are included), we measure the branching fraction $\mathcal{B}(B_s^0 \rightarrow D_s^- \pi^+) = (0.68 \pm 0.22 \pm 0.16)\%$. The systematic error includes the $N_{5S}^{b\bar{b}}$ and f_s uncertainties and the uncertainty of $\sim 14\%$ in the reconstruction efficiency, which is dominated by the uncertainty in the value of

$\mathcal{B}(D_s^- \rightarrow \phi \pi^-)$. This branching fraction is consistent with the value $\mathcal{B}(B_s^0 \rightarrow D_s^- \pi^+) = (0.38 \pm 0.05 \pm 0.14)\%$ derived from a CDF measurement of $\mathcal{B}(B_s^0 \rightarrow D_s^- \pi^+)/\mathcal{B}(B^0 \rightarrow D^- \pi^+)$ [27] using the 2006 PDG values of the $B^0 \rightarrow D^- \pi^+$ and $D_s^- \rightarrow \phi \pi^-$ branching fractions [28].

M_{bc} and ΔE scatterplots are also obtained for the $B_s^0 \rightarrow D_s^{*-} \pi^+$ (Fig. 2(b)) and $B_s^0 \rightarrow D_s^{(*)-} \rho^+$ (Fig. 2(c)) decay modes. We observe four $B_s^0 \rightarrow D_s^{*-} \pi^+$ candidates and seven $B_s^0 \rightarrow D_s^{(*)-} \rho^+$ candidates in the $B_s^* \bar{B}_s^*$ channel, one $B_s^0 \rightarrow D_s^{(*)-} \rho^+$ candidate in the $B_s^* \bar{B}_s^0 + B_s^0 \bar{B}_s^*$ channel, and no candidates in the $B_s^0 \bar{B}_s^0$ channel.

The scatterplot in M_{bc} and ΔE for the $B_s^0 \rightarrow J/\psi \phi$ and $B_s^0 \rightarrow J/\psi \eta$ decays is shown in Fig. 2(d). Two candidates are reconstructed in the $B_s^0 \rightarrow J/\psi \phi$ mode and one candidate is reconstructed in the $B_s^0 \rightarrow J/\psi \eta$ mode. One of the observed $B_s^0 \rightarrow J/\psi \phi$ candidates is reconstructed in the $J/\psi \rightarrow \mu^+ \mu^-$ mode and one in the $J/\psi \rightarrow e^+ e^-$ mode. As a cross-check, the branching fraction $\mathcal{B}(B_s^0 \rightarrow J/\psi \phi) = (0.9 \pm 0.6 \pm 0.2) \times 10^{-3}$ is obtained for these two candidates, which agrees with the CDF measurement [29] within the large errors. The numbers of B_s^0 candidates reconstructed in the $D_s^- \pi^+$, $D_s^- \rho^+$, $D_s^{*-} \pi^+$, $D_s^{*-} \rho^+$, $J/\psi \phi$, and $J/\psi \eta$ decay modes and lying in the signal region corresponding to the $B_s^* \bar{B}_s^*$ channel are listed in Table I. In addition, the numbers of events reconstructed in the three D_s^- decay modes are shown separately.

Although the M_{bc} and ΔE signal resolutions are slightly different for different decay modes, for simplicity in Fig. 2 the same size elliptical signal regions are shown for all modes. Because of low statistics, a small variation of signal shape for different B_s^0 decays can be neglected in the M_{bc} and ΔE measurements discussed below. It is, however, included in the systematic uncertainties.

The six B_s^0 modes shown in Fig. 2 are combined to increase the statistical significance of the B_s^0 signal.

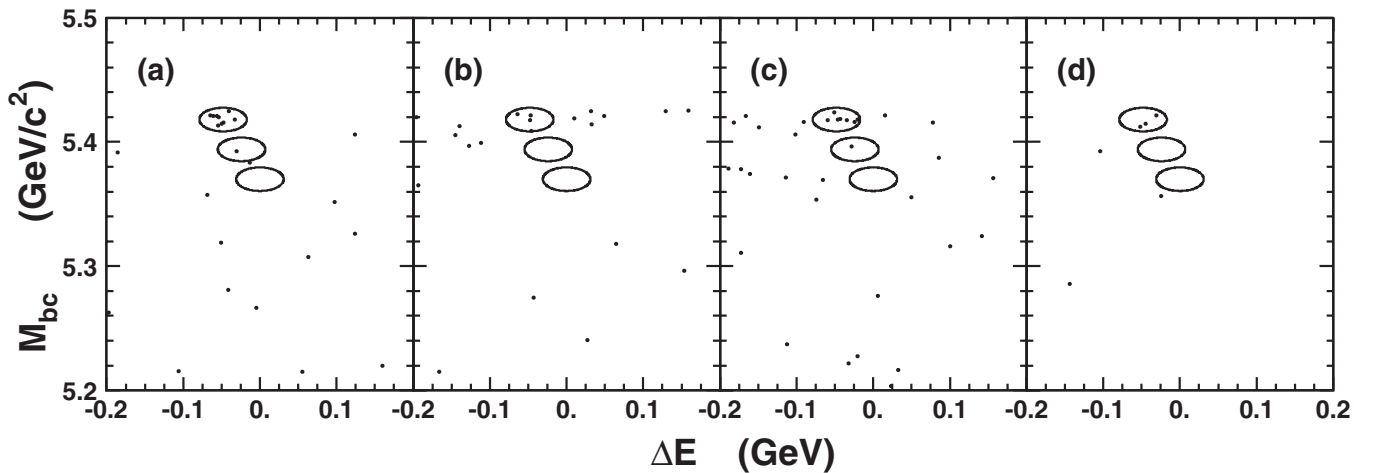


FIG. 2. The M_{bc} and ΔE scatter plots for the (a) $B_s^0 \rightarrow D_s^- \pi^+$, (b) $B_s^0 \rightarrow D_s^{*-} \pi^+$, (c) $B_s^0 \rightarrow D_s^{(*)-} \rho^+$, and (d) $B_s^0 \rightarrow J/\psi \phi$ and $B_s^0 \rightarrow J/\psi \eta$ decay modes.

TABLE I. The number of the B_s^0 candidates located within the elliptical signal region corresponding to the $B_s^* \bar{B}_s^*$ channel. The events reconstructed in the $D_s^- \rightarrow \phi \pi^-$, $D_s^- \rightarrow K^{*0} K^-$, and $D_s^- \rightarrow K_S^0 K^-$ decay modes are listed separately.

Decay mode	$D_s^- \rightarrow \phi \pi^-$	$K^{*0} K^-$	$K_S^0 K^-$	Sum
$B_s^0 \rightarrow D_s^- \pi^+$	4	2	3	9
$B_s^0 \rightarrow D_s^{*-} \pi^+$	2	1	1	4
$B_s^0 \rightarrow D_s^- \rho^+$	2	1	0	3
$B_s^0 \rightarrow D_s^{*-} \rho^+$	2	2	0	4
$B_s^0 \rightarrow J/\psi \phi$				2
$B_s^0 \rightarrow J/\psi \eta$				1

Distributions in ΔE are obtained separately for events from three M_{bc} intervals, $5.408 \text{ GeV}/c^2 < M_{bc} < 5.429 \text{ GeV}/c^2$ (Fig. 3(a)), $5.384 \text{ GeV}/c^2 < M_{bc} < 5.405 \text{ GeV}/c^2$ (Fig. 3(b)), and $5.360 \text{ GeV}/c^2 < M_{bc} < 5.380 \text{ GeV}/c^2$ (Fig. 3(c)), corresponding to B_s^0 production proceeding through the $B_s^* \bar{B}_s^*$, $B_s^* \bar{B}_s^0 + B_s^0 \bar{B}_s^*$, or $B_s^0 \bar{B}_s^0$ channels, respectively.

Each of these three distributions is fitted with the sum of a Gaussian to describe the signal and a linear function to describe the background. In the $B_s^* \bar{B}_s^*$ channel (Fig. 3(a)), the width and the peak position are allowed to float, and their values $\sigma_{\Delta E} = (10.2 \pm 1.9) \text{ MeV}$ and $\langle \Delta E \rangle = (-47.6 \pm 2.6) \text{ MeV}$, respectively, are obtained from the fit. The width agrees with the value of $\sim 12 \text{ MeV}$ obtained from a MC simulation of the dominant $B_s^0 \rightarrow D_s^- \pi^-$ decay channel. Because of low statistics in the other two distributions, the peak positions and widths are fixed. The widths are taken from MC simulations. The peak position is fixed to zero for the $B_s^0 \bar{B}_s^0$ channel and that for the $B_s^* \bar{B}_s^0 + B_s^0 \bar{B}_s^*$ channel is fixed to -23.8 MeV , which is half of the value obtained for the $\langle \Delta E \rangle$ peak position in the $B_s^* \bar{B}_s^*$ channel. The fits yield 20.3 ± 4.8 events and 1.5 ± 2.0 events for the $B_s^* \bar{B}_s^*$ and $B_s^* \bar{B}_s^0 + B_s^0 \bar{B}_s^*$ channels, respectively; no events are observed in the $B_s^0 \bar{B}_s^0$ channel. From these numbers and approximately equal B_s^0 reconstruction efficiency in these three channels found in

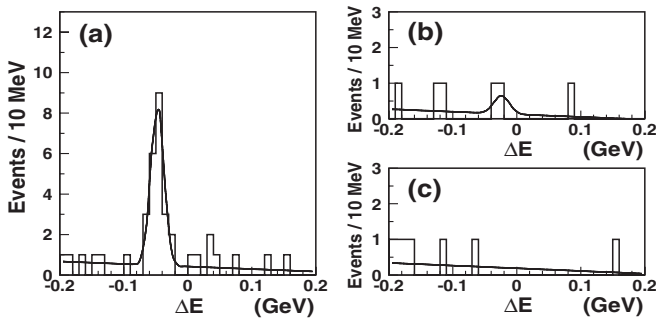


FIG. 3. The ΔE distributions for B_s^0 candidates with (a) $5.408 \text{ GeV}/c^2 < M_{bc} < 5.429 \text{ GeV}/c^2$, (b) $5.384 \text{ GeV}/c^2 < M_{bc} < 5.405 \text{ GeV}/c^2$, and (c) $5.360 \text{ GeV}/c^2 < M_{bc} < 5.380 \text{ GeV}/c^2$, corresponding to B_s^0 production through the $B_s^* \bar{B}_s^*$, $B_s^* \bar{B}_s^0 + B_s^0 \bar{B}_s^*$, and $B_s^0 \bar{B}_s^0$ channels, respectively. Curves represent the results of the fits described in the text.

MC simulation, we obtain the ratio $\sigma(e^+ e^- \rightarrow B_s^* \bar{B}_s^*) / \sigma(e^+ e^- \rightarrow B_s^{(*)} \bar{B}_s^{(*)}) = (93_{-9}^{+7} \pm 1)\%$ at the $Y(5S)$ energy. The first uncertainty is statistical and the second uncertainty is systematic, dominated by uncertainties in the fit procedure. Potential models predict the fraction of $B_s^* \bar{B}_s^*$ production to be around 70% [30–32].

The B_s^* mass can be extracted from the fit to the M_{bc} distribution of the observed events in the $B_s^* \bar{B}_s^*$ channel. In this channel the M_{bc} variable, calculated from the formula $M_{bc} = \sqrt{(E_{\text{beam}}^{\text{CM}})^2 - (p_{B_s^0}^{\text{CM}})^2}$, is equal, to a good approximation, to the mass of the B_s^* meson. This follows from the fact that the difference between the B_s^0 and B_s^* momenta is statistically unbiased from zero and is smaller than the experimental resolution in B_s^0 momentum. Figure 4 shows the M_{bc} distribution of the candidates in the range $-80 \text{ MeV} < \Delta E < -20 \text{ MeV}$, where signal events from the $B_s^* \bar{B}_s^*$ production channel are expected. We fit this distribution with the sum of a Gaussian to describe the signal and a so-called ARGUS function [33] to describe the background. The fit yields a mass value of $M(B_s^*) = (5418 \pm 1 \pm 3) \text{ MeV}/c^2$. The large systematic error is dominated by the uncertainty in the collider beam energy calibration resulting in a $e^+ e^-$ CM beam energy uncertainty of $\sim 3 \text{ MeV}$. The uncertainty of the method used to determine the $M(B_s^*)$ mass is estimated by MC simulation to be around $0.5 \text{ MeV}/c^2$. The uncertainty in the particle momenta measurements translated to the $M(B_s^*)$ mass uncertainty is also around $0.5 \text{ MeV}/c^2$. The observed width of the B_s^* signal is $(3.6 \pm 0.6) \text{ MeV}/c^2$ and agrees with the value obtained from the MC simulation, which assumes zero natural width and is dominated by the KEKB energy spread. The obtained B_s^* mass is 1.8σ higher than the value measured recently by CLEO [34], $M(B_s^*) = (5411.7 \pm 1.6 \pm 0.6) \text{ MeV}/c^2$.

Using the measured values of the B_s^* mass and the energy difference $\langle \Delta E \rangle = (-47.6 \pm 2.6) \text{ MeV}$, we can calculate the B_s^0 mass. The value $\langle \Delta E \rangle$ is the mean energy

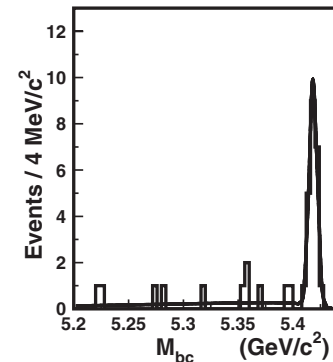


FIG. 4. The B_s^* mass distribution for events within the $-80 \text{ MeV} < \Delta E < -20 \text{ MeV}$ interval, where the B_s^0 signal from the $B_s^* \bar{B}_s^*$ channel is expected. Curve represents the result of the fit described in the text.

difference between the B_s^* and B_s^0 mesons in the CM system and, in a good approximation, is equal to the mass difference of the B_s^* and B_s^0 mesons. The photon energy in the $B_s^* \rightarrow B_s^0 \gamma$ decay is a constant in the B_s^* rest frame, and the smearing due to the Lorentz transformation from the B_s^* rest frame to the CM rest frame is small compared with the central value of the photon energy. Finally we obtain a mass value of $M(B_s^0) = (5370 \pm 1 \pm 3) \text{ MeV}/c^2$. The second uncertainty in the B_s^0 mass value is the systematic uncertainty dominated by the statistical uncertainty on the $\langle \Delta E \rangle$ measurement, which will improve once more statistics become available. The uncertainty due to the collider beam energy calibration almost linearly affects both the $M(B_s^*)$ and $\langle \Delta E \rangle$ values and nearly cancels in the $M(B_s^0)$ mass calculations. Other systematic uncertainties affecting the B_s^0 mass are similar to those in the B_s^* mass measurement and are small. The obtained B_s^0 mass agrees well with the PDG value, $M(B_s^0) = (5369.6 \pm 2.4) \text{ MeV}/c^2$ [28], and the most recent CDF measurement, $M(B_s^0) = (5366.01 \pm 0.73 \pm 0.33) \text{ MeV}/c^2$ [35].

IV. SEARCH FOR $B_s^0 \rightarrow \gamma\gamma$, $B_s^0 \rightarrow \phi\gamma$, $B_s^0 \rightarrow K^+K^-$, AND $B_s^0 \rightarrow D_s^{(*)+}D_s^{(*)-}$ DECAYS

Distributions in M_{bc} and ΔE are also obtained for the reconstructed $B_s^0 \rightarrow \gamma\gamma$ (Fig. 5(a)), $B_s^0 \rightarrow \phi\gamma$ (Fig. 5(b)), $B_s^0 \rightarrow K^+K^-$ (Fig. 5(c)), and $B_s^0 \rightarrow D_s^{(*)+}D_s^{(*)-}$ (Fig. 5(d)) candidates. Only the B_s^0 signal regions corresponding to the dominant $B_s^*\bar{B}_s^*$ channel are considered for the searches reported here. These regions are wider for the $B_s^0 \rightarrow \phi\gamma$ and $B_s^0 \rightarrow \gamma\gamma$ decays, where energy losses due to photon radiation lead to a large tail at lower values of ΔE . The signal region for the $B_s^0 \rightarrow D_s^{(*)+}D_s^{(*)-}$ search is slightly smaller, because of the kinematics of the decay to two

heavy particles. The shapes of the signal regions for these decays are optimized from the MC simulation.

To avoid multiple D_s^* and D_s cross-channel candidates, only one candidate per event is selected in the $B_s^0 \rightarrow D_s^{(*)+}D_s^{(*)-}$ analysis, where the number of multiple candidates can be rather large. The candidate with the M_{bc} value closest to the nominal $M(B_s^*)$ value measured above is chosen. No significant signals are observed in any of the distributions shown in Fig. 5. However one $B_s^0 \rightarrow \phi\gamma$ event, two $B_s^0 \rightarrow K^+K^-$ events, and one $B_s^0 \rightarrow D_s^{*+}D_s^{*-}$ event lie within the signal regions, whereas backgrounds outside the signal regions are not large. The numbers of events within the signal regions, the estimated background contributions, the efficiencies, and the upper limits for the corresponding B_s^0 branching fractions are listed in Table II. For comparison, the previously published upper limits and branching fractions are also shown. The numbers of events and the upper limits are obtained using only the B_s signal region corresponding to the $B_s^*\bar{B}_s^*$ channel. The upper limits are obtained using the Feldman-Cousins method [36], and a small correction due to systematic uncertainties is applied. The efficiencies are determined from the MC simulation. The number of initial $B_s^*\bar{B}_s^*$ pairs is obtained by multiplying the number of $B_s^{(*)}\bar{B}_s^{(*)}$ pairs measured in the inclusive analysis [2] by the production ratio of $B_s^*\bar{B}_s^*$ pairs to all $B_s^{(*)}\bar{B}_s^{(*)}$ pairs obtained in this analysis. We calculated the previous $B_s^0 \rightarrow D_s^+D_s^-$ branching fraction listed in Table II using the measurement $\mathcal{B}(B_s^0 \rightarrow D_s^+D_s^-)/\mathcal{B}(B^0 \rightarrow D_s^+D^-) = 1.67 \pm 0.41 \pm 0.47$ from CDF [22] and the $\mathcal{B}(B^0 \rightarrow D_s^+D^-)$ value from the PDG [28].

The upper limit obtained for the decay $B_s^0 \rightarrow \gamma\gamma$ is about 3 times smaller than the most restrictive published limit [8]. However, it is still 2 orders of magnitude above SM predictions [10,11]. The upper limit obtained for $B_s^0 \rightarrow \phi\gamma$ is about a factor of ten larger than the theoretically ex-

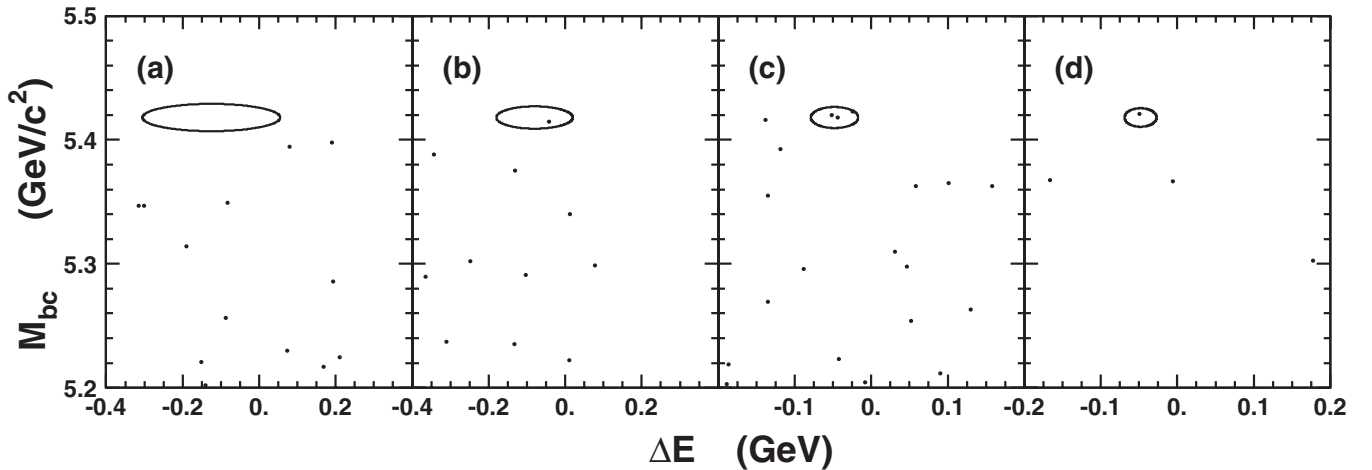


FIG. 5. The scatter plots in M_{bc} and ΔE for the (a) $B_s^0 \rightarrow \gamma\gamma$, (b) $B_s^0 \rightarrow \phi\gamma$, (c) $B_s^0 \rightarrow K^+K^-$, and (d) $B_s^0 \rightarrow D_s^{(*)+}D_s^{(*)-}$ decay modes. In the latter case, the signal event is reconstructed in the $B_s^0 \rightarrow D_s^{*+}D_s^{*-}$ decay mode, while the three background events are reconstructed in the $B_s^0 \rightarrow D_s^+D_s^-$ decay mode. The ellipses indicate the B_s^0 signal regions for the $B_s^*\bar{B}_s^*$ channel.

TABLE II. The number of events in the signal region (Yield), the estimated background contribution (Background), the efficiencies, the 90% C.L. upper limits derived in this analysis (Belle upper limit) and previously published upper limits or branching fractions (Previous UL/BF) for the $B_s^0 \rightarrow \gamma\gamma$, $B_s^0 \rightarrow \phi\gamma$, $B_s^0 \rightarrow K^+K^-$ and $B_s^0 \rightarrow D_s^{(*)+}D_s^{(*)-}$ decay modes.

Decay mode	Yield (events)	Background (events)	Efficiencies (%)	Belle upper limit	Previous UL/BF
$B_s^0 \rightarrow \gamma\gamma$	0	0.5	20.0	$<0.53 \times 10^{-4}$	$<1.48 \times 10^{-4}$ [8]
$B_s^0 \rightarrow \phi\gamma$	1	0.15	5.9	$<3.9 \times 10^{-4}$	$<1.2 \times 10^{-4}$ [9]
$B_s^0 \rightarrow K^+K^-$	2	0.16	9.8	$<3.1 \times 10^{-4}$	$(3.30 \pm 0.57 \pm 0.67) \times 10^{-5}$ [19]
$B_s^0 \rightarrow D_s^+D_s^-$	0	0.02	0.020	$<6.7\%$	$(1.09 \pm 0.27 \pm 0.47)\%$ [22]
$B_s^0 \rightarrow D_s^{*+}D_s^-$	1	0.01	0.0099	$<12.1\%$...
$B_s^0 \rightarrow D_s^{*+}D_s^{*-}$	0	<0.01	0.0052	$<25.7\%$...

pected branching fraction [37]. The upper limit obtained for the $B_s^0 \rightarrow K^+K^-$ decay is an order of magnitude larger than the value measured by CDF [19]. For SM branching fractions, statistically significant signals of ~ 10 events can be obtained for the $B_s^0 \rightarrow \phi\gamma$ and $B_s^0 \rightarrow K^+K^-$ modes in a $\sim 30 \text{ fb}^{-1}$ dataset on the $Y(5S)$.

The upper limits obtained for $B_s^0 \rightarrow D_s^{(*)+}D_s^{(*)-}$ decays are of special interest because the $D_s^{(*)+}D_s^{(*)-}$ states are expected to be dominantly CP eigenstates. Assuming that the branching fractions for the $D_s^+D_s^-$, $D_s^{*+}D_s^-$, $D_s^+D_s^{*-}$, and $D_s^{*+}D_s^{*-}$ final states are each in the range (1–3)%, we expect about 5–10 events in each of these four channels with statistics of $\sim 30 \text{ fb}^{-1}$. Within the SM framework such measurements can provide an important constraint on the value of $\Delta\Gamma_{B_s^0}/\Gamma_{B_s^0}$ [20,21].

V. CONCLUSIONS

Several exclusive B_s^0 decays are reconstructed using 1.86 fb^{-1} of data taken at the $Y(5S)$ resonance with the Belle detector at the KEKB asymmetric energy e^+e^- collider.

B_s^0 signals are found in six decay modes: $B_s^0 \rightarrow D_s^{(*)-}\pi^+$, $B_s^0 \rightarrow D_s^{(*)-}\rho^+$, $B_s^0 \rightarrow J/\psi\phi$, and $B_s^0 \rightarrow J/\psi\eta$. The branching fraction $\mathcal{B}(B_s^0 \rightarrow D_s^- \pi^+) = (0.68 \pm 0.22 \pm 0.16)\%$ is measured. Combining the studied six channels, we observe a significant B_s^0 signal and obtain the masses $M(B_s^0) = (5370 \pm 1 \pm 3) \text{ MeV}/c^2$ and $M(B_s^*) = (5418 \pm 1 \pm 3) \text{ MeV}/c^2$. B_s^0 production through the $B_s^* \bar{B}_s^*$ channel is found to dominate over other $B_s^{(*)} \bar{B}_s^{(*)}$ channels; the ratio $\sigma(e^+e^- \rightarrow B_s^* \bar{B}_s^*)/\sigma(e^+e^- \rightarrow B_s^{(*)} \bar{B}_s^{(*)}) = (93_{-9}^{+7} \pm 1)\%$ is measured. These results are in agreement with CLEO measurements [7].

We have also searched for $B_s^0 \rightarrow \gamma\gamma$, $B_s^0 \rightarrow \phi\gamma$, $B_s^0 \rightarrow K^+K^-$, and $B_s^0 \rightarrow D_s^{(*)+}D_s^{(*)-}$ decay modes and set upper limits on their branching fractions. The upper limit on $B_s^0 \rightarrow \gamma\gamma$ is 3 times more restrictive than the best existing

limit. The background levels in these decays are low, indicating that the sensitivity of future studies of these decays with larger statistics will not be limited by backgrounds. We expect that significant signals for $B_s^0 \rightarrow K^+K^-$, $B_s^0 \rightarrow \phi\gamma$, and $B_s^0 \rightarrow D_s^{(*)+}D_s^{(*)-}$ decays can be observed in $\sim 30 \text{ fb}^{-1}$ of data. With such statistics the upper limit for the $B_s^0 \rightarrow \gamma\gamma$ decay should provide an important constraint on some BSM models.

ACKNOWLEDGMENTS

We thank the KEKB group for the excellent operation of the accelerator, the KEK cryogenics group for the efficient operation of the solenoid, and the KEK computer group and the National Institute of Informatics for valuable computing and Super-SINET network support. We acknowledge support from the Ministry of Education, Culture, Sports, Science, and Technology of Japan and the Japan Society for the Promotion of Science; the Australian Research Council and the Australian Department of Education, Science, and Training; the National Science Foundation of China and the Knowledge Innovation Program of the Chinese Academy of Sciences under Contract No. 10575109 and IHEP-U-503; the Department of Science and Technology of India; the BK21 program of the Ministry of Education of Korea, the CHER SRC program and Basic Research program (Grant No. R01-2005-000-10089-0) of the Korea Science and Engineering Foundation, and the Pure Basic Research Group program of the Korea Research Foundation; the Polish State Committee for Scientific Research; the Ministry of Education and Science of the Russian Federation and the Russian Federal Agency for Atomic Energy; the Slovenian Research Agency; the Swiss National Science Foundation; the National Science Council and the Ministry of Education of Taiwan; and the U.S. Department of Energy.

- [1] M. Artuso *et al.* (CLEO Collaboration), Phys. Rev. Lett. **95**, 261801 (2005).
- [2] A. Drutskoy *et al.* (Belle Collaboration), Phys. Rev. Lett. **98**, 052001 (2007).
- [3] V. Papadimitriou, Fermilab Report No. FERMILAB-CONF-05-497-E, 2005.
- [4] G. Gomez-Ceballos, Fermilab Report No. FERMILAB-CONF-05-495-E, 2005.
- [5] A. Abashian *et al.* (Belle Collaboration), Nucl. Instrum. Methods Phys. Res., Sect. A **479**, 117 (2002).
- [6] S. Kurokawa and E. Kikutani, Nucl. Instrum. Methods Phys. Res., Sect. A **499**, 1 (2003), and other papers included in this volume.
- [7] G. Bonvicini *et al.* (CLEO Collaboration), Phys. Rev. Lett. **96**, 022002 (2006).
- [8] M. Acciarri *et al.* (L3 Collaboration), Phys. Lett. B **363**, 137 (1995).
- [9] D. Acosta *et al.* (CDF Collaboration), Phys. Rev. D **66**, 112002 (2002).
- [10] L. Reina, G. Ricciardi, and A. Soni, Phys. Rev. D **56**, 5805 (1997).
- [11] S. W. Bosch and G. Buchalla, J. High Energy Phys. **08** (2002) 054.
- [12] A. Gemintern, S. Bar-Shalom, and G. Eilam, Phys. Rev. D **70**, 035008 (2004).
- [13] W. J. Huo, C. D. Lu, and Z. J. Xiao, BIHEP Report No. BIHEP-TH-2003-6, 2003.
- [14] R. Fleischer, Phys. Lett. B **459**, 306 (1999).
- [15] A. Khodjamirian, T. Mannel, and M. Melcher, Phys. Rev. D **68**, 114007 (2003).
- [16] D. London and J. Matias, Phys. Rev. D **70**, 031502(R) (2004).
- [17] A. J. Buras, R. Fleischer, S. Recksiegel, and F. Schwab, Nucl. Phys. **B697**, 133 (2004).
- [18] S. Baek, D. London, J. Matias, and J. Virto, J. High Energy Phys. **02** (2006) 027.
- [19] A. Abulencia *et al.* (CDF Collaboration), Phys. Rev. Lett. **97**, 211802 (2006).
- [20] Y. Grossman, Phys. Lett. B **380**, 99 (1996).
- [21] I. Dunietz, R. Fleischer, and U. Nierste, Phys. Rev. D **63**, 114015 (2001).
- [22] S. Farrington *et al.* (CDF Collaboration), Fermilab Report No. FERMILAB-CONF-06-405-E.
- [23] E. Nakano, Nucl. Instrum. Methods Phys. Res., Sect. A **494**, 402 (2002).
- [24] K. Hanagaki *et al.*, Nucl. Instrum. Methods Phys. Res., Sect. A **485**, 490 (2002).
- [25] A. Abashian *et al.*, Nucl. Instrum. Methods Phys. Res., Sect. A **491**, 69 (2002).
- [26] G. C. Fox and S. Wolfram, Phys. Rev. Lett. **41**, 1581 (1978).
- [27] A. Abulencia *et al.* (CDF Collaboration), Phys. Rev. Lett. **96**, 191801 (2006).
- [28] W.-M. Yao *et al.* (Particle Data Group), J. Phys. G **33**, 1 (2006).
- [29] F. Abe *et al.* (CDF Collaboration), Phys. Rev. D **54**, 6596 (1996).
- [30] N. Byers and D. S. Hwang, UCLA-87-TEP-44, 1987.
- [31] D. M. J. Lovelock *et al.* (CUSB Collaboration), Phys. Rev. Lett. **54**, 377 (1985).
- [32] J. Lee-Franzini *et al.* (CUSB Collaboration), Phys. Rev. Lett. **65**, 2947 (1990).
- [33] H. Albrecht *et al.* (ARGUS Collaboration), Phys. Lett. B **229**, 304 (1989).
- [34] O. Aquines *et al.* (CLEO Collaboration), Phys. Rev. Lett. **96**, 152001 (2006).
- [35] D. Acosta *et al.* (CDF Collaboration), Phys. Rev. Lett. **96**, 202001 (2006).
- [36] G. J. Feldman and R. D. Cousins, Phys. Rev. D **57**, 3873 (1998).
- [37] N. Barik, S. Kar, and P. C. Dash, Phys. Rev. D **57**, 405 (1998).